

# A Densely Connected Convolutional Network Towards Efficient Recognition of Intracranial Hemorrhage Using CT Images

Md. Harun Or Rashid<sup>1</sup>, Boshir Ahmed<sup>2</sup>

1 Department of CSE, Bangladesh Army University of Engineering & Technology (BAUET), Qadirabad, Natore, Rajshahi, Bangladesh  
2 Department of CSE, Rajshahi University of Engineering & Technology (RUET), Rajshahi, Bangladesh

\*Corresponding author's email:  
harun.ruetbd@gmail.com

Received: 27/05/2022  
Accepted: 27/09/2022  
Published: 13/07/2024

Data Availability: The data are available on request from the corresponding author.

Competing Interests: The authors declare that they have no known competing financial interests or personal relationships that could have appeared to influence the work reported in this paper.

DOI: 10.3329/gubjse.v9i1.74880

Copyright: © GUBJSE copyright related information.

## Abstract

Intracranial Bleeding also known as Intracranial Hemorrhage (ICH) is a severe issue for human beings and the most common cause of it is trauma. Majorly ICH occurs due to hypertension and around 2.5 per 10,000 people get affected by one of its subtypes. The human brain consists of lots of soft tissue and nerves, that's why it is so tough to find affected areas within the shortest period and to apply proper treatment or medication for a radiologist by analyzing the Computed Tomography (CT) images. In addition to ICH treatment being expensive, a densely connected convolutional network (DenseNet-169) model is recommended to accurately detect the damaged region quickly and affordably to facilitate the treatment of the patient. All were private and inaccessible, with the exception of the CQ500 and the Radiological Society of North America (RSNA) datasets about ICH. In our study, we employed stage-2 of the RSNA dataset, which comprises 121,232 test images and 752,803 training images. Phase-1 and phase-2 are the two stages of the dataset. Among the various preprocessing techniques, image type conversion, resizing, and normalization were performed on the dataset. During the learning phase of our model, for hyper-tuning, a portion (30%) of training data was utilized as validation data. The test data was then used to evaluate the model's efficacy, and it was found that the ICH recognition accuracy of our developed model was 98%. Index Terms— Intracranial Hemorrhage, CT images, DenseNet, Training, Testing, Recognition, RSNA.

**Keywords:** Intracranial Hemorrhage, CT images, DenseNet, Training, Testing, Recognition, RSNA.

## Highlights

- DenseNet-169 achieves 98% accuracy in identifying intracranial hemorrhage
- RSNA dataset with 121,232 test images and 752,803 training images is utilized.
- Addresses the challenge of quickly and affordably detecting damaged brain regions.

## Acknowledgements

This paper and the research behind it would not have been possible without the financial and laboratory supports of the Department of Computer Science and Engineering at the Bangladesh Army University of Engineering & Technology.

## 1 Introduction

Bleeding within the brain or skull is the cause of intracranial hemorrhage, also known as intracerebral hemorrhage (ICH). The brain has a great deal of soft tissue and is capable of bleeding both within as well as outside of these tissues. For a better understanding of the internal structure, the following figure (Fig. 1) shows a cross-section of the brain representing the cranial meninges.

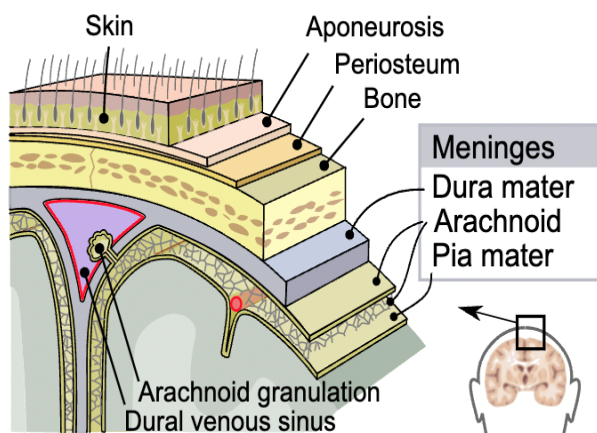


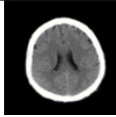
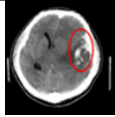
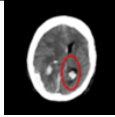
Fig 1. Structure of cranial meninges

Depending on where the bleeding began, there are five different types of ICH: epidural (EDH), subdural (SDH), subarachnoid (SAH), intraparenchymal (IPH), and intraventricular (IVH). The types of hemorrhage as well as their location, source, presentation, and other details are shown in the tables below (TABLE 1 and TABLE 2). Within the last 4-5 years several pieces of research had been accomplished on ICH recognition and classification but most of them were on private datasets collected from specific hospital, clinic, or diagnostic center.

On the RSNA and CQ500 datasets, a few studies had been conducted employing a variety of widely used algorithms, including VGG-16, CNN, LSTM, ResNet50, Xception, InceptionResNetV2, and InceptionV3. In majority of the study, feature extraction and classification were carried out independently using machine learning algorithms and CNN respectively, which was time-consuming and comparably less effective in terms of accuracy and ROC-AUC value.

Our research makes a recommendation for a DenseNet model with 169 layers, called DenseNet-169, to help patients and radiologists in recognition and classification of ICH so that the abnormality of the affected person can be diagnosed quickly, cheaply, and more efficiently.

Table 1. Intra-axial hemorrhage with normal one

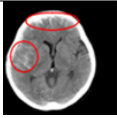
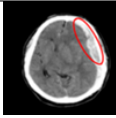
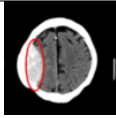
Parameters	Normal	Intraparenchymal	Intraventricular
Location	————	Inside of the brain	Inside of the ventricle
Imaging			
Mechanism	————	Arteriovenous malformation, malignancy, high blood pressure, trauma, etc	Possibly linked to intraparenchymal and subarachnoid hemorrhages
Source	————	Vascular or arterial	Vascular or arterial
Presentation	————	Acute (unexpected headache, nausea and vomiting)	Acute (unexpected headache, nausea and vomiting)

## 2 Literature Review

Several classification systems have been proposed to categorize ICH based on various factors, including location, size, and underlying causes. The researchers used just machine learning methods in the early stages of ICH identification. Deep learning methods are now widely employed in medical image analysis, including ICH recognition and classification. In a recent study, Manikandan Rajagopal et al. [1] focused on the implementation of hybrid deep neural networks for cerebral hemorrhage detection. Their research established Conv-LSTM, a type of hybrid deep learning system that combines long short-term memory (LSTM) with convolution neural networks (CNNs) having an accuracy of 95.14%.

Xception, InceptionV3, InceptionResNetV2, ResNet50, VGG16, and Xception were the five deep learning models that Mohammed Ammar et al. [2] compared using the RSNA dataset. Based on the obtained results, the VGG-16 architecture performed 96% more accurately than the other models. A variety of techniques developed using machine learning as well as deep learning were used in several studies [2]–[12] to help radiologists diagnose the ICH and its different types more quickly. The researchers in [13]

**Table 2.** Extra-axial hemorrhage

Parameters	Subarachnoid	Subdural	Epidural
Location	Between the arachnoid and the pia mater	Between the Dura and the arachnoid	Between the dura and the skull
Imaging			
Mechanism	Arteriovenous malformations or rupture of aneurysms or trauma	Trauma	Trauma or after surgery
Source	Predominantly arterial	Venous (bridging veins)	Arterial
Presentation	Acute (worst headache of life)	May be insidious (worsening headache)	Acute (skull fracture and altered mental status)

proposed a combination of a convolutional neural network model (CNN) along with a long short-term memory (LSTM) technique to aid in the detection and classification of ICH, which achieved a loss in the range of 0.07528 as a multi-label logarithmic (or 93%–94% in accuracy). A research project that employed computed tomography (CT) scans to automatically detect and test for trauma-related brain lesions was also completed by Vidhya V. et al. [14]. The model, developed in [15], had an AUC of 0.94 and was designed to automatically identify radiological data with minimal effort and expenditure. The researchers used a combination of an LSTM, a 1D CNN, and a logistic function in order to achieve the performance. In a study, Ajay Patel et al. [16] created a hybrid network that included CNN with bidirectional LSTM in the same year, and the achieved ROC-AUC value was 0.96. Another study by Sui Paul Ang et al. [17] had been accomplished on the segmentation of human brain tissue. They developed a batch-by-batch deep learning algorithm in their study to segment the tissue of the human brain, and the approach was able to reach 84.04% of the expected classification rate. Numerous researchers conducted surveys and reviews of the literature in [18]–[21] on the topic of ICH recognition. They shared the information they gathered as well as

helpful recommendations. In our study, we attempted to improve recognition and classification performance in the shortest amount of time, despite the existence of numerous studies on ICH, in order to benefit radiologists and patients.

### 3 Proposed Methodology

We suggest an approach that is comprised of several key steps connected in a sequential fashion. The flow chart (Fig. 2) illustrates our suggested methodology’s flow pattern.

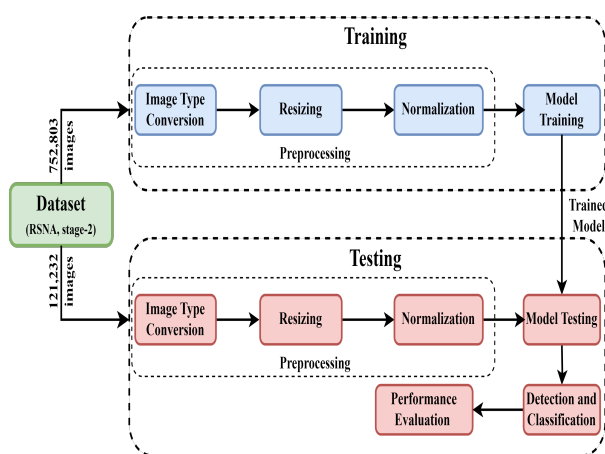


**Fig 2.** Flow diagram of proposed methodology

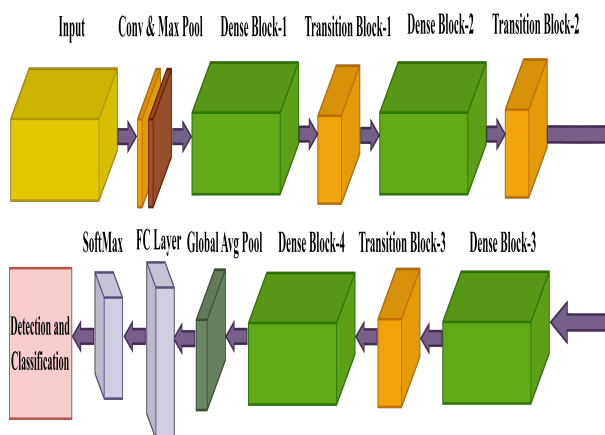


**Fig 3.** Block diagram of our implemented model

DenseNet-169 was utilized to identify and classify ICH, which was the aim of our experiment. The accompanying

diagram (Fig. 3) shows the operating framework of the deployed model.

According to the working flow, the model receives images that have been preprocessed as input and runs them through a sequence of dense blocks (which include several convolutional layers) and transition blocks (which include a batch normalization, a rectified linear unit, an average layer of pooling as well as a convolutional layer). In order to provide the desired result, our developed model processes the result obtained from the most recent dense block (Dense Block-4) using the layer that is fully connected, softmax operation, and a global average pooling layer. The accompanying table (TABLE 3) shows the internal organization of our implemented model.

**Table 3.** Internal architecture of implemented model

Layers	Output Size	DenseNet-169
Convolution	112×112	7×7 conv, stride 2
Pooling	56×56	3×3 max pool, stride 2
Dense Block-1	56×56	$\left\{ \begin{array}{l} 1 \times 3 \text{ conv} \\ 3 \times 3 \text{ conv} \end{array} \right\} \times 6$
Transition Layer 1	56×56	1×1 conv
	28×28	2×2 average pool, stride 2
Dense Block-2	28×28	$\left\{ \begin{array}{l} 1 \times 3 \text{ conv} \\ 3 \times 3 \text{ conv} \end{array} \right\} \times 12$
Transition Layer 2	28×28	1×1 conv
	14×14	2×2 average pool, stride 2
Dense Block-3	14×14	$\left\{ \begin{array}{l} 1 \times 3 \text{ conv} \\ 3 \times 3 \text{ conv} \end{array} \right\} \times 32$
Transition Layer 3	14×14	1×1 conv
	7×7	2×2 average pool, stride 2
Dense Block-4	7×7	$\left\{ \begin{array}{l} 1 \times 3 \text{ conv} \\ 3 \times 3 \text{ conv} \end{array} \right\} \times 32$
Classification	1×1	7×7 global average pool
	1000	1000D fully connected, softmax

### 3.1 Input Image

The RSNA phase-2 datasets were utilized in the research we conducted, and the initial image size was 512×512×3 which is reduced to 224×224×3 by the resizing operation to feed by DenseNet-169.

### 3.2 Convolution and Max Pooling Layer

A neural network made up of convolutional neurons is mostly made up of the convolution layer. This layer compares the output image with a limited set of filters or kernels to carry out the convolution operation. Finally, the layer takes the most noticeable features from the given input image and outputs a feature map. The feature map gets smaller depending on the layer of max pooling. The graphic below (Fig. 4) illustrates a 3×3 maximum pooling operation with stride 2.

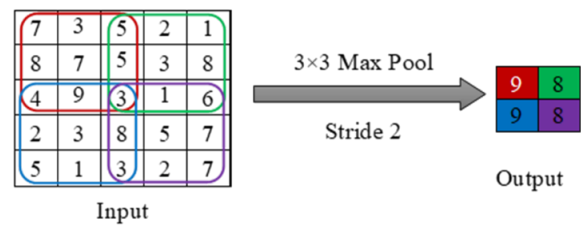


**Fig 4.** Max pooling operation

Only the maximum values are selected by this operation and thus the image gets sharpened since the most significant features are retrieved.

### 3.3 Dense Block

The uniformity of size required for the feature map is an essential part of the interconnectivity between each convolution layer inside a dense block. The dense block is taken into account as a module by us. In the model that we recommended, there were four dense blocks: Dense Block-1, Dense Block-2, Dense Block-3, and Dense Block-4. The accompanying figure (Fig. 5) illustrates the layer-to-layer interconnectivity inside a densely packed block.

Once all of the layers that have come before within a dense block have been successively concatenated, the resultant feature maps can be expressed using the following equation:

$$x_l = H_l ([x_0, x_1, x_2, \dots, x_{l-1}]) \tag{1}$$

The attributes, index, and non-linear function of the  $l$ th layer are represented by the symbols  $x_l$ ,  $H_l$  and  $l$ , in this instance.

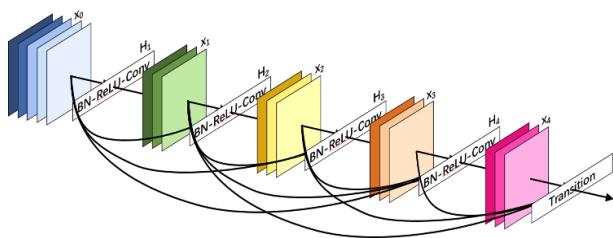


Fig 5. A dense block of three layers growing at a rate of  $k=3$  [18]

### 3.4 Transition Block

A block consisting of convolution, average pooling, rectified linear unit, and batch normalization is referred to as a transition block. A transition block's structure is depicted in the below figure (Fig. 6).

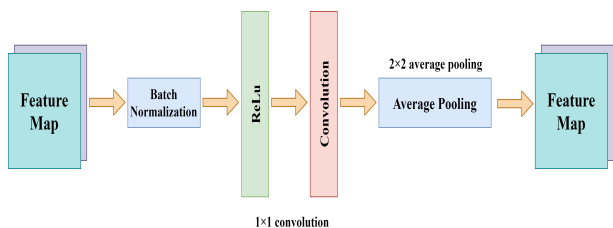


Fig 6. Architectural design of a transition block

The feature maps are down sampled using blocks that are situated in between two consecutive dense blocks. Transition Blocks-1, 2, and 3 are the three transition blocks that our model makes use of.

### 3.5 Global Average Pooling

Numerous deep learning and machine learning algorithms frequently suffer from the over fitting issue. In order to solve this issue, fewer parameters must be used, which calls for the use of a pooling operation. With the goal of reducing dimensionality, the pooling of global averages (GAP) is an operation of pooling that keeps going unless it attains one dimension in space.

### 3.6 Fully Connected Layer

In our implemented model, the fully connected also known as FC layer, which is an essential component of CNN architecture, is placed adjacent to the layer of the pooling of global average. This layer learns to associate the identified

features with a specific label after the features are separated. Every neuron in the layer is linked to each of the other neurons above and below, much like in an artificially generated neural network (ANN).

### 3.7 Softmax Function

A kind of activation function that is widely used in the last layer of multi-class classification is the normalized exponential function, frequently referred to as a softmax function or softargmax. It takes a row of CNN outputs and turns it into a probability vector.

## 4 Results and Discussion

The phase-2 of RSNA dataset, which was obtained from Kaggle, was used in our investigation. In our dataset, there were 107933 aberrant data points in the train part.

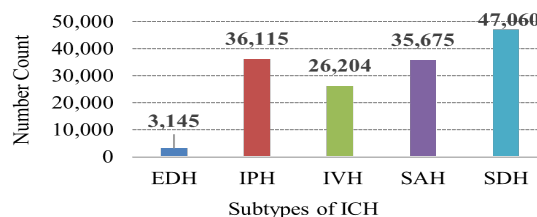
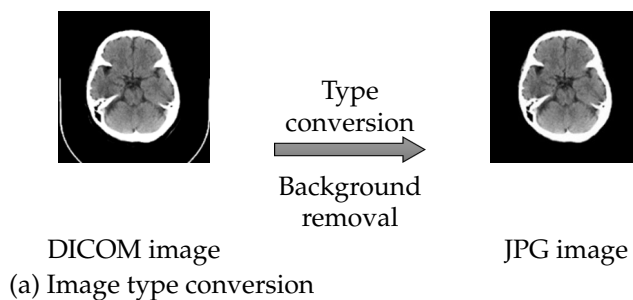


Fig 7. Bar graph for subtypes of ICH with exact count

Considering an initial rate of learning of  $1.25 \times 10^{-4}$ , the model that we suggested had been trained for 50 epochs. The type-wise ICH data with an exact count is shown in the above figure (Fig. 7). Preprocessing methods such as image type conversion, resizing, and normalization are employed on the data before using it as input for the model. The resulting images from all of the actions performed are displayed in the corresponding figure (Fig. 8 (a), (b) and (c) respectively).



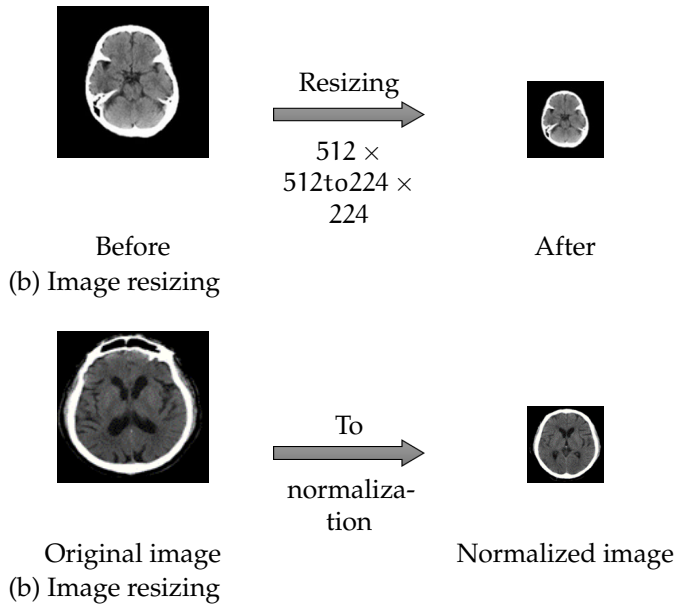


Fig 8. Preprocessing operation.

To perform well, a model needs to be properly trained during the training phase. The accuracy and loss metrics are used to assess a classifier’s performance. Fig. 9 and Fig. 10 display the efficiency of our implemented method during the training phase respectively.

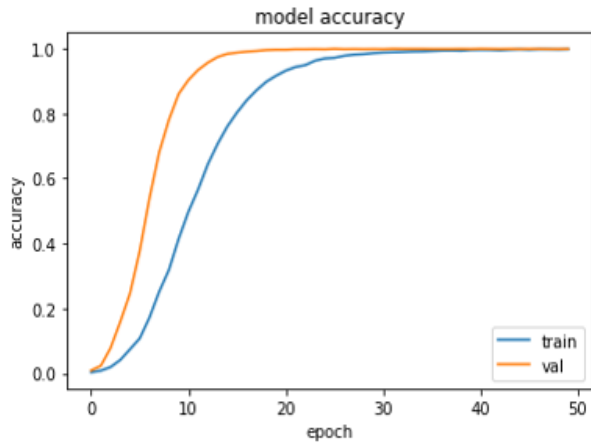


Fig 9. Train vs. validation accuracy curve

Numerous metrics, such as weighted average, accuracy, macro, and micro averages, are used to evaluate the performance of a multi-class classification task. The values of true positives (TP), true negatives (TN), false positives (FP), and false negatives (FN) were used to calculate the results for precision, recall, and f1-score. Our implemented model yields the following set of matrices of confusion for every ICH subtype, shown in Fig. 11 (a), (b), (c), (d) and

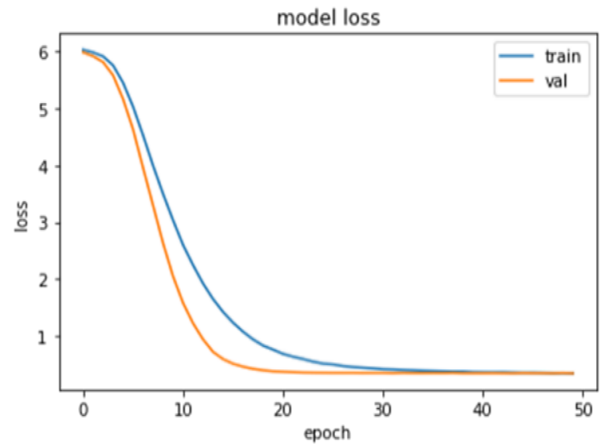
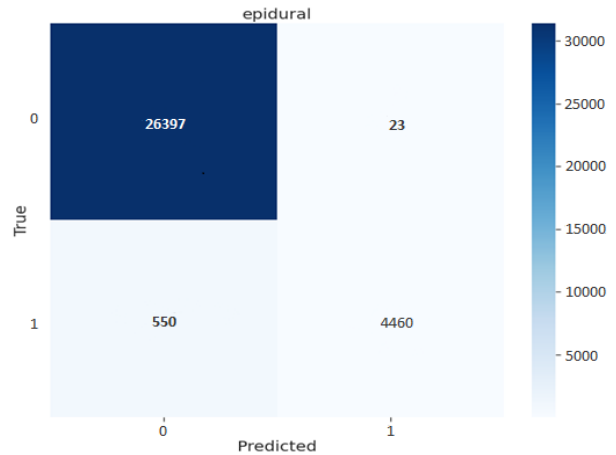
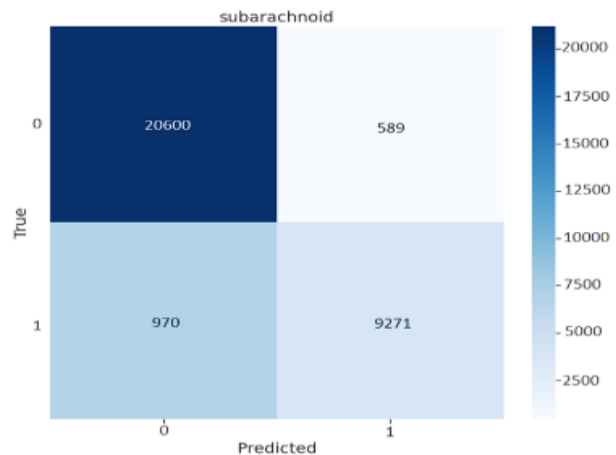


Fig 10. Train vs. validation loss curve

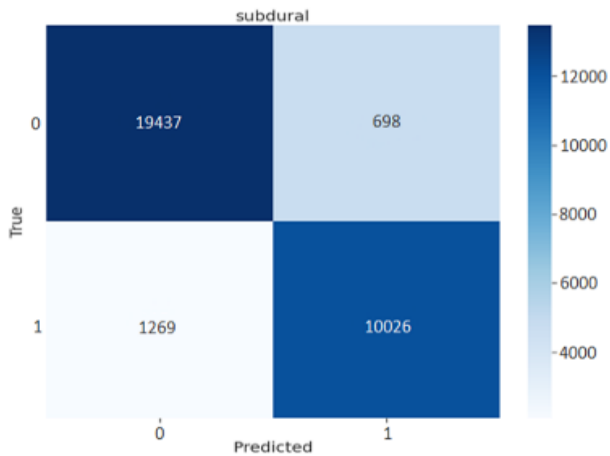
(e) respectively.



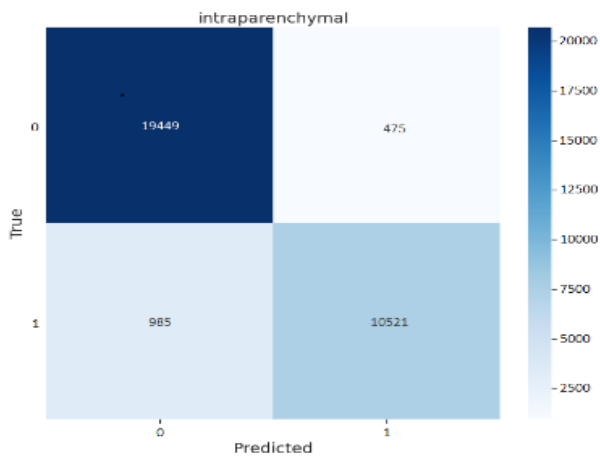
(a)Epidural hemorrhage



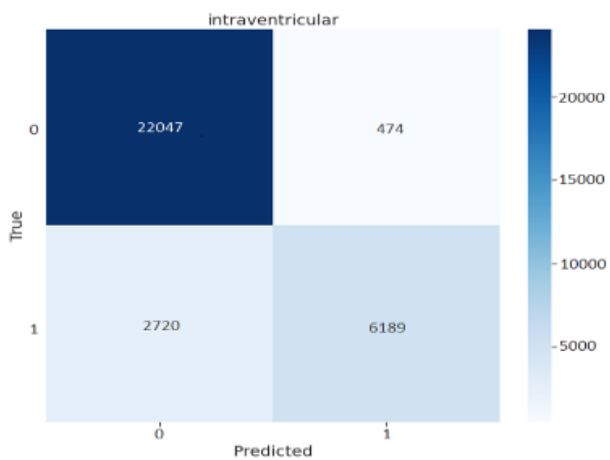
(b)Subarachnoid hemorrhage



(c)Subdural hemorrhage



(d)Intraparenchymal hemorrhage



(e)Intraventricular hemorrhage

Fig 11. Confusion matrices for ICH subtypes

The effectiveness of our suggested approach are shown in TABLE 4 and Fig. 12 respectively

Table 4. Performance metrics for densenet -169

Parameters	Precision	Recall	F1-score	Support
epidural	0.99	0.89	0.94	5010
intraparenchymal	0.96	0.91	0.94	11506
intraventricular	0.93	0.91	0.92	8909
subarachnoid	0.94	0.91	0.92	10241
subdural	0.93	0.89	0.91	11295
accuracy			0.98	46961
micro avg	0.95	0.86	0.90	46961
macro avg	0.95	0.90	0.93	46961
weighted avg	0.95	0.90	0.92	46961

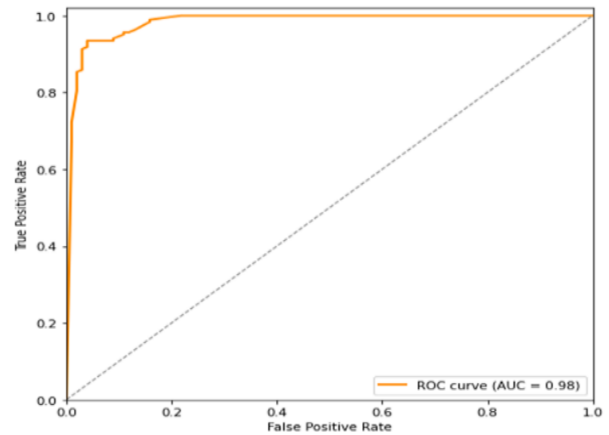


Fig 12. ROC curve for DenseNet-169

The following formulas are used to determine the evaluation metrics for the recommended model:

$$\text{precision} = \frac{TP}{TP + FP} \tag{2}$$

$$\text{recall} = \frac{TP}{TP + FN} \tag{3}$$

$$\text{F1 - score} = \frac{2 \times \text{precision} \times \text{recall}}{\text{precision} + \text{recall}} \tag{4}$$

$$\left. \begin{aligned} &\text{Micro avg (precision)} \\ &= \frac{\sum TP}{\sum TP + \sum FP} \\ &\text{Micro avg (recall)} \\ &= \frac{\sum TP}{\sum TP + \sum FN} \\ &\text{Micro avg (f1 - score)} \\ &= \frac{2 \times \sum \text{precision} \times \sum \text{recall}}{\sum \text{precision} + \sum \text{recall}} \end{aligned} \right\}$$

$$\left. \begin{aligned} \text{Macro avg (precision)} &= \frac{\sum \text{precision}}{\text{No. of class}} \\ \text{Macro avg (recall)} &= \frac{\sum \text{recall}}{\text{No. of class}} \\ \text{Macro avg (f1 - score)} &= \frac{\sum \text{f1 - score}}{\text{No. of class}} \end{aligned} \right\}$$

$$\left. \begin{aligned} &\text{Weighted avg (precision)} \\ &= \frac{\sum \text{precision} \times \text{support}}{\sum \text{support}} \\ &\text{Weighted avg (recall)} \\ &= \frac{\sum \text{recall} \times \text{support}}{\sum \text{support}} \\ &\text{Weighted avg (f1 - score)} \\ &= \frac{\sum \text{f1 - score} \times \text{support}}{\sum \text{support}} \end{aligned} \right\}$$

TABLE 5 and Fig. 13 below represent a comparison between our obtained results and those of other comparable works respectively.

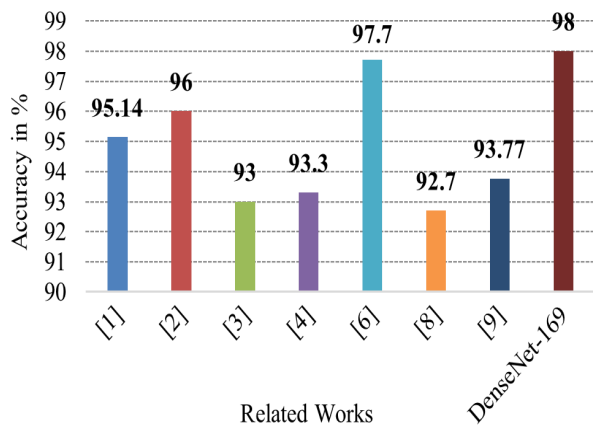


Fig 13. Comparison of related works with DenseNet-169

Table 5. Comparison of related works

	Authors	Applied Model	Accuracy
(5)	Manikandan Rajagopal et al. [1]	Conv-LSTM	95.14%
	Mohammed Ammar et al. [2]	VGG-16	96.00%
	Ko Hoon et al. [3]	CNN-LSTM	93.00%
	Tomasz Lewick et al. [4]	ResNet-50	93.30%
	Muhammad Asif et al. [6]	Res-Inc-LGBM	97.70%
(6)	Luis Cortés-Ferre et al. [8]	Grad-CAM	92.70%
	Maryam Wardah et al. [9]	Inception, ResNet-V2 and ResNet-50	93.77%
	DenseNet-169 model	DenseNet-169	98.00%

### 5 Conclusion

(7) In this study, an architecture for deep learning called DenseNet-169 was used to address the recognition as well as classification problem on ICH CT scans. Convolutional Neural Network (CNN) and Long Short Term Memory (LSTM) techniques were almost universally employed by researchers to carry out their investigations and generate the necessary data. Without it, a large number of them had to make use of proprietary datasets that weren't accessible to the public. The fact that there was still a research gap and an opportunity to enhance the efficacy of ICH identification and categorization with its subtypes, despite the abundance of available data, motivated us to carry out this work. Our proposed model can achieve better results (Fig. 16) on RSNA stage-2 dataset in the area of ICH recognition and classification. In the future, we hope to develop a software that can identify ICH and categorize different types of ICH in addition to applying our suggested approach to other ICH datasets.

### References

[1] M. Rajagopal, S. Buradagunta, M. Almeshari, Y. Alzamil, R. Ramalingam, and V. Ravi, "An efficient framework to detect intracranial hemorrhage using hybrid deep neural networks," *Brain Sciences*, vol. 13, no. 3, p. 400, 2023.



- [2] M. Ammar, M. A. Lamri, S. Mahmoudi, and A. Laidi, "Deep learning models for intracranial hemorrhage recognition: A comparative study," *Procedia Computer Science*, vol. 196, pp. 418–425, 2022.
- [3] H. Ko, H. Chung, H. Lee, and J. Lee, "Feasible study on intracranial hemorrhage detection and classification using a cnn-lstm network," in *2020 42nd Annual International Conference of the IEEE Engineering in Medicine & Biology Society (EMBC)*, IEEE, 2020, pp. 1290–1293.
- [4] T. Lewick, M. Kumar, R. Hong, and W. Wu, "Intracranial hemorrhage detection in ct scans using deep learning," in *2020 IEEE Sixth International Conference on Big Data Computing Service and Applications (BigDataService)*, IEEE, 2020, pp. 169–172.
- [5] K. Jnawali, M. R. Arbabshirani, A. E. Ulloa, N. Rao, and A. A. Patel, "Automatic classification of radiological report for intracranial hemorrhage," in *2019 IEEE 13th international conference on semantic computing (ICSC)*, IEEE, 2019, pp. 187–190.
- [6] M. Asif, M. A. Shah, H. A. Khattak, *et al.*, "Intracranial hemorrhage detection using parallel deep convolutional models and boosting mechanism," *Diagnostics*, vol. 13, no. 4, p. 652, 2023.
- [7] M. López-Pérez, A. Schmidt, Y. Wu, R. Molina, and A. K. Katsaggelos, "Deep gaussian processes for multiple instance learning: Application to ct intracranial hemorrhage detection," *Computer Methods And Programs In Biomedicine*, vol. 219, p. 106783, 2022.
- [8] L. Cortés-Ferre, M. A. Gutiérrez-Naranjo, J. J. Egea-Guerrero, S. Pérez-Sánchez, and M. Balcerzyk, "Deep learning applied to intracranial hemorrhage detection," *Journal of Imaging*, vol. 9, no. 2, p. 37, 2023.
- [9] M. Wardah, M. Mateen, T. S. Malik, *et al.*, "Automated brain hemorrhage classification and volume analysis," *CMC-COMPUTERS MATERIALS & CONSTRUCTION*, vol. 75, no. 1, pp. 2283–2299, 2023.
- [10] Y. Li, J. Wu, H. Li, *et al.*, "Automatic detection of the existence of subarachnoid hemorrhage from clinical ct images," *Journal of medical systems*, vol. 36, pp. 1259–1270, 2012.
- [11] J. Sengupta and R. Alzbutas, "Intracranial hemorrhages segmentation and features selection applying cuckoo search algorithm with gated recurrent unit," *Applied Sciences*, vol. 12, no. 21, p. 10851, 2022.
- [12] L. C. Ascanio, G. A. Maragos, B. C. Young, M. D. Boone, and E. M. Kasper, "Spontaneous intracranial hemorrhage in pregnancy: A systematic review of the literature," *Neurocritical care*, vol. 30, pp. 5–15, 2019.
- [13] N. T. Nguyen, D. Q. Tran, N. T. Nguyen, and H. Q. Nguyen, "A cnn-lstm architecture for detection of intracranial hemorrhage on ct scans," *medRxiv*, pp. 2020–04, 2020.
- [14] A. Gudigar, U. Raghavendra, A. Hegde, *et al.*, "Automated detection and screening of traumatic brain injury (tbi) using computed tomography images: A comprehensive review and future perspectives," *International journal of environmental research and public health*, vol. 18, no. 12, p. 6499, 2021.
- [15] M. Vidya, A. H. Shastry, and Y. Mallya, "Automated detection of intracranial hemorrhage in noncontrast head computed tomography," in *Advances in Computational Techniques for Biomedical Image Analysis*, Elsevier, 2020, pp. 71–98.
- [16] A. Patel, S. C. Van De Leemput, M. Prokop, B. Van Ginneken, and R. Manniesing, "Image level training and prediction: Intracranial hemorrhage identification in 3d non-contrast ct," *Ieee Access*, vol. 7, pp. 92355–92364, 2019.
- [17] S. P. Ang, S. L. Phung, M. M. Schira, A. Bouzerdoum, and S. T. M. Duong, "Human brain tissue segmentation in fmri using deep long-term recurrent convolutional network," in *2018 Digital Image Computing: Techniques and Applications (DICTA)*, IEEE, 2018, pp. 1–7.
- [18] G. Huang, Z. Liu, L. Van Der Maaten, and K. Q. Weinberger, "Densely connected convolutional networks," in *Proceedings of the IEEE conference on computer vision and pattern recognition*, 2017, pp. 4700–4708.
- [19] M. D. Jørgensen, R. Antulov, S. Hess, and S. Lysdahlgaard, "Convolutional neural network performance compared to radiologists in detecting intracranial hemorrhage from brain computed tomography: A systematic review and meta-analysis," *European journal of radiology*, vol. 146, p. 110073, 2022.
- [20] M. A. Correa, S. Cardona, L. L. Fernández, *et al.*, "Implementation of the infrascanner in the detection of post-traumatic intracranial bleeding: A narrative review," *Brain Disorders*, vol. 5, p. 100026, 2022.
- [21] T. Shibata, N. Hashimoto, and M. Mase, "Intracranial hemorrhage in posterior reversible encephalopathy syndrome due to corticosteroid pulse therapy," *Brain Disorders*, vol. 7, p. 100040, 2022.



**Md. Harun Or Rashid** was born in Rangpur, Bangladesh, in 1995. He received the Bachelor of Science, B.Sc. Engineering in Computer Science & Engineering (CSE) from the Rajshahi University of Engineering & Technology (RUET), Rajshahi, Bangladesh, in 2017 and the Master of Science, M.Sc. Engineering in

Computer Science & Engineering (CSE) from the Rajshahi University of Engineering & Technology (RUET), Rajshahi, Bangladesh, in October 2023. He has published more than 10 research papers in different national and international journals and conferences. Currently, he is working as a Lecturer in the Department of CSE, Bangladesh Army University of Engineering & Technology (BAUET) since October 2018. His research interests include image processing, machine learning, and data mining.



**Boshir Ahmed** is a Dhaka native and he is working as a faculty member in the department of Computer Science & Engineering (CSE), Rajshahi University of Engineering & Technology (RUET) since 24th June 2001. In addition to this role, he is professor of this Department, with research interests in image/video analysis and Computer vision. In

this service period, he took active part in postgraduate & undergraduate academic programs of this department and also have got the opportunity to conduct and supervise different research projects. He received the Bachelor of Science, B.Sc. Engineering in Computer Science & Engineering (CSE) from the Dhaka University of Engineering & Technology (DUET), Gazipur, Bangladesh, in 2001, the Master of Science, M.Sc. Engineering in Computer Science & Engineering (CSE) from the Rajshahi University of Engineering & Technology (RUET), Rajshahi, Bangladesh, in 2012 and the Doctor of Philosophy, PhD in Computer Science & Engineering (CSE) from the Rajshahi University of Engineering & Technology (RUET), Rajshahi, Bangladesh, in 2015. He served as a Head at the Department of CSE in RUET. So far, he has published more than 5 book chapters, 17 national and international journal papers and 52 conference papers.